## SUPPLEMENTAL METHODS

### MTS assay

To quantify viable cells in the cytotoxicity assays we used CellTiter 96® $AQ_{ueous}$ One Solution Reagent (Promega, Madison, WI). Cells were plated at 100 µl/well of the 96-well plate, at the following numbers: 500-1000 cells/well for the CHO AA8 cells, 250-500 cells/well for the MDA-MB-231-BR3 cells, and 1000 cells/well for the HCC1806, SUM149, HCC1937 and its derivatives. Cells were allowed to attach overnight. Next day, cells were quality checked to ensure that cells were attached and divided. Dynasore, tubulin binders and other modifiers of chlorambucil effect were added 30 min - 1 hour before addition of chlorambucil. Cell viability was quantified in 5 days by adding 10 µl of the CellTiter reagent and measuring absorbance at 490nm with a 96-well plate reader after incubation for 2 and 4 hours at 37oC.

### High-throughput chemical screen

CHO AA8 cells were plated onto clear-bottomed/black-walled 384 well plates (E&K Scientific, Santa Clara, CA) at 150 cells/well using a Matrix Wellmate dispenser (Thermo Scientific, Sunnyvale, CA), and chlorambucil and chemical library compounds were added using fully automated liquid handling system Sciclone ALH3000 (Caliper Life Sciences, Waltham, MA), and plates were held at 37°C/5% $CO_2$ for 96 hr. Cell viability was assessed 4 hr after the addition of CellTiter-Blue reagent (Promega, Madison, WI) using Analyst GT (Molecular Devices, Sunnyvale, CA) plate reader with an excitation of 555 nm and emission of 590 nm. Average Z' factor values in our assay were 0.56, indicating that the assay was very robust. Out of more than 130,000 uncharacterized compounds 640 were tested positive in the initial screen out of which 46 were confirmed in a dose response assay to potentiate chlorambucil cytotoxicity. These compounds were re-tested for chlorambucil sensitivity dose-response analysis, and if confirmed,

were analyzed for their ability to inhibit formation of radiation-induced Rad51 foci and gene conversion.

**Orthotopic xenograft model**

Cell pellets from MDA-MB-231-BR3 cell lines expressing doxycycline-inducible shDNM2 or shGFP were washed with cold PBS, and resuspended in ice-cold Matrigel (BD Biosciences). 8-week old female Nu/Nu mice (088, Charles River Laboratories) were anesthetized by inhalation of 2% isoflurane and injected ($0.5\times10^6$ cells in 0.1 ml) using a 27½ gauge needle into the fat pad located under the left side of the 4$^{th}$ inguinal mammary gland. After 10 days, when the tumors reached 60–90 mm$^3$ the mice were randomly distributed into treatment groups (n=9 for the drug-treated and n=8 for vehicle-treated). Treatment consisted of 2 cycles of cyclophosphamide or one cycle of cisplatin (300 mg/kg/cycle or 16 mg/kg/cycle, respectively). Cyclophosphamide cycle was comprised of three I.P. injections given every other day followed by 2-week rest period. Cisplatin was given by I.P. injections on days 11, 13, 15 and 17 after tumor cells inoculations. To induce DNM2 knockdown doxycycline was given 3 days before and during cyclophosphamide or cisplatin administration. Tumor size and body weight measurements were carried out every other day. Tumor size measurements were performed by caliper using the formula $V=d^2D/2$ for the tumor volume estimation, where $d$ and $D$ are the shortest and longest diameters of tumor, respectively.

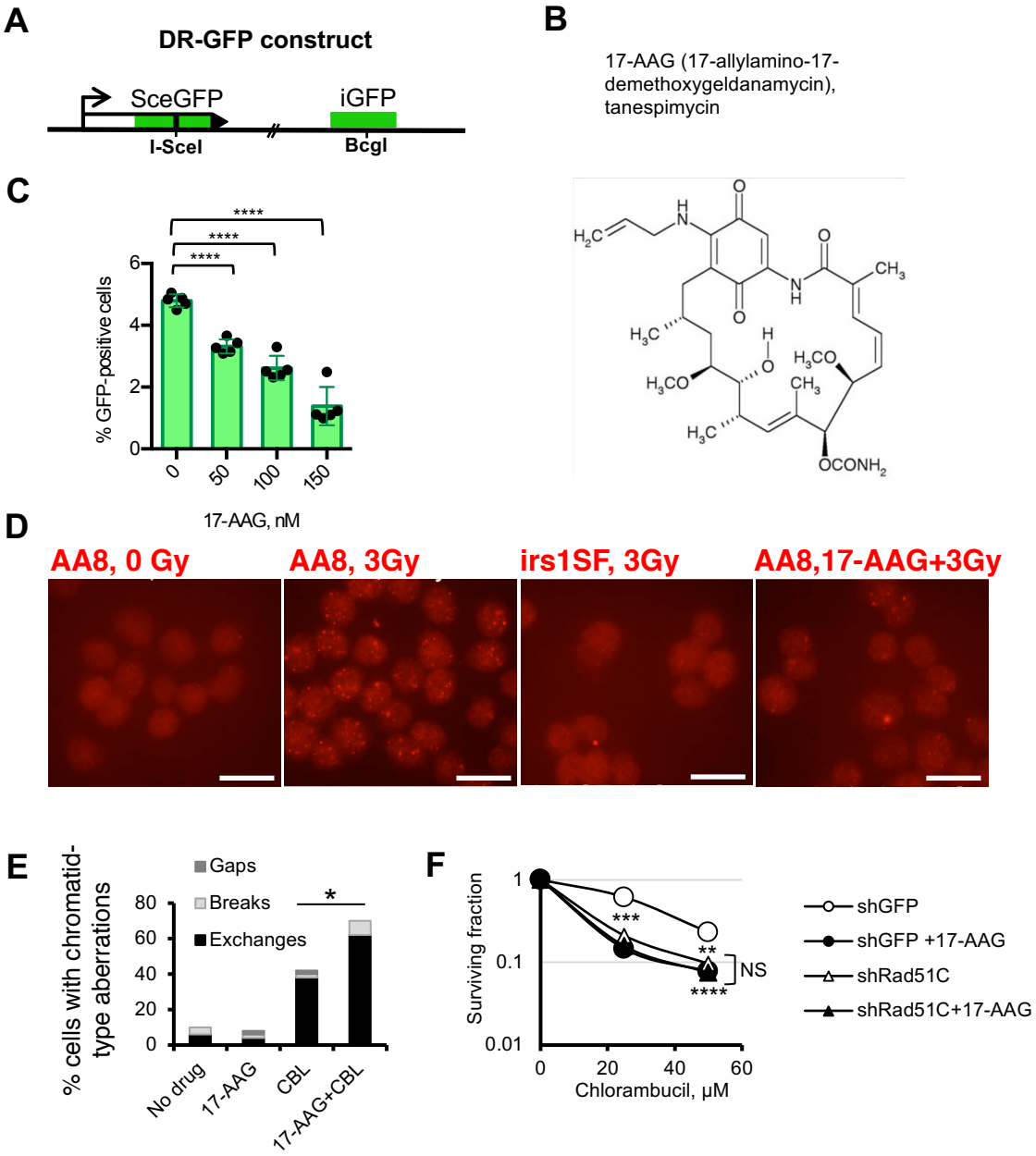


**Supplemental Figure 1. 17-allylamino-17-demethoxygeldanamycin (17-AAG) acts as an inhibitor of homology-directed repair. (A)** The recombination reporter DR-GFP is stably integrated into the genome of U2OS osteosarcoma cell line (adapted from 64). *SceGFP* is a *GFP* gene that contains an I-SceI endonuclease site within the coding region. Cleavage of the I-SceI site in vivo and repair by homologous recombination using the downstream *iGFP* repeat as a template restores expression of GFP. **(B)** 17-AAG is an analog of geldanamycin. **(C)** 17-AAG treatment reduces gene conversion frequency in U2OS-DR-GFP cells, in which a DNA double-strand break was introduced after transfection with I-SceI. Values are means ± SDs from n = 3 experiments. Representative flow charts are shown in Figure 1B. Significance analysis: ANOVA. **(D)** 17-AAG inhibits formation of Rad51 foci in the CHO AA8 cells after 3 Gy. Cells were fixed 2 hours post-irradiation. Note the absence of Rad51 foci in unirradiated CHO AA8 cells and in HR-deficient CHO irs1SF cells after 3 Gy. Representative images from n ≥ 3 experiments are shown. Scale bar is 20 μm. Quantitation is provided in Figure 2D. **(E)** The same data as in Figure 1D show the representation of different categories of chromatid-type aberrations in each treatment group. **(F)** Knockdown of Rad51C increases sensitivity to chlorambucil in AA8 cells. 17-AAG (100 μM) does not increase chlorambucil sensitivity of the Rad51C knockdown cells. Non-specific knockdown of GFP (shGFP) was used as a control. Shown are means ± SDs (ranges) from n≥2 MTS assays. Significance analysis: two-way ANOVA.
*, p <0.05, **, p < 0.01; ***, p < 0.001; ****, p < 0.0001.

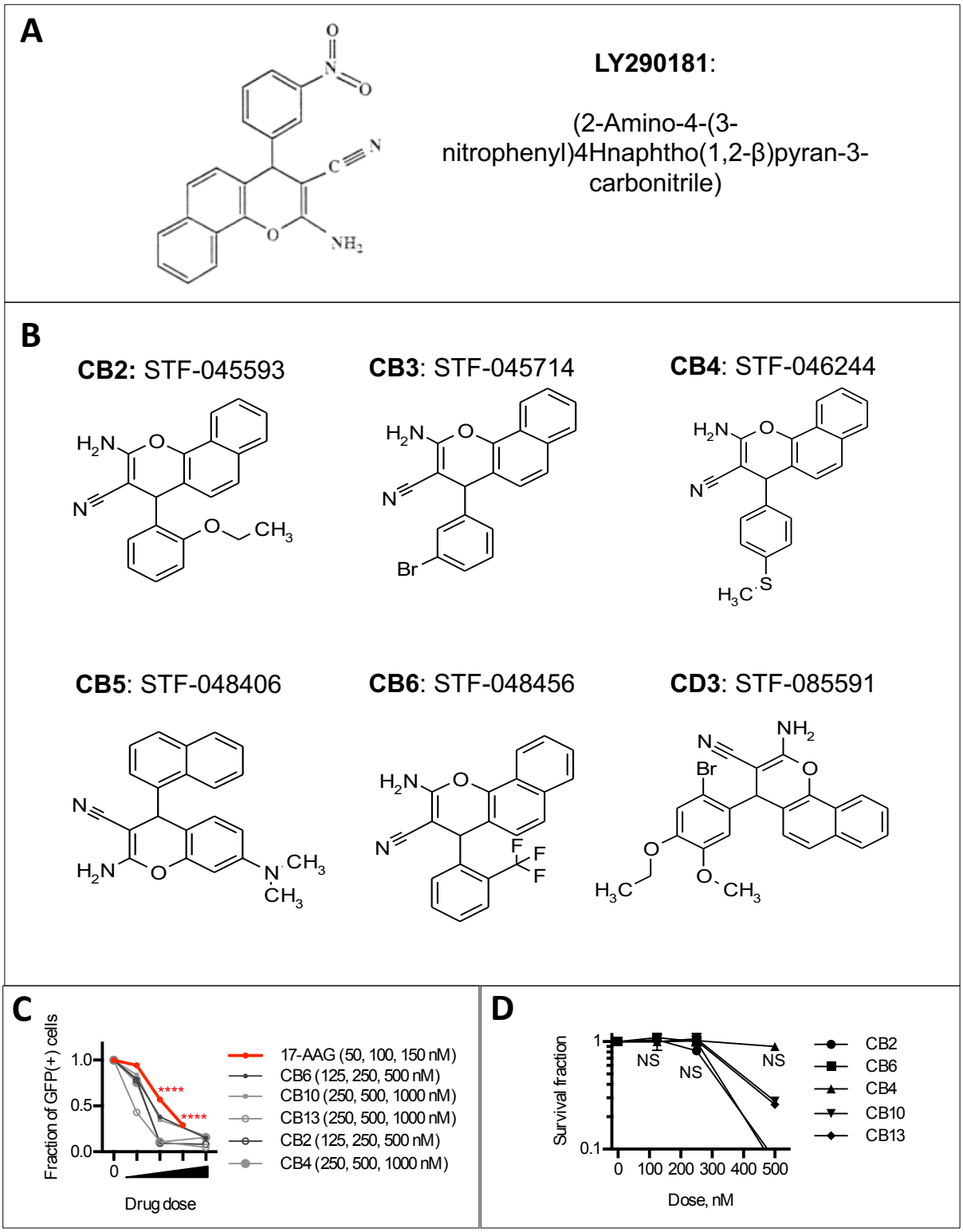


**Supplemental Figure 2.** **(A)** Chemical structures of LY290181 and **(B)** its derivatives (CB2, CB3, CB4, CB5, CB6, and CD3), which were among positive hits in a screen for compounds increasing sensitivity of mammalian cells to the DNA cross-linking agent chlorambucil. **(C)** LY290181 derivatives inhibit gene conversion at concentrations compatible with cell survival **(**CB2 and CB6 were used at concentrations 125 and 250 nM and CB4, CB10 and CB13 – at 250 and 500 nM). 17-AAG was used as a positive control. P< 0.0001, ANOVA. **(D)** Tubulin binders inhibit gene conversion at concentrations below those affecting cell survival.

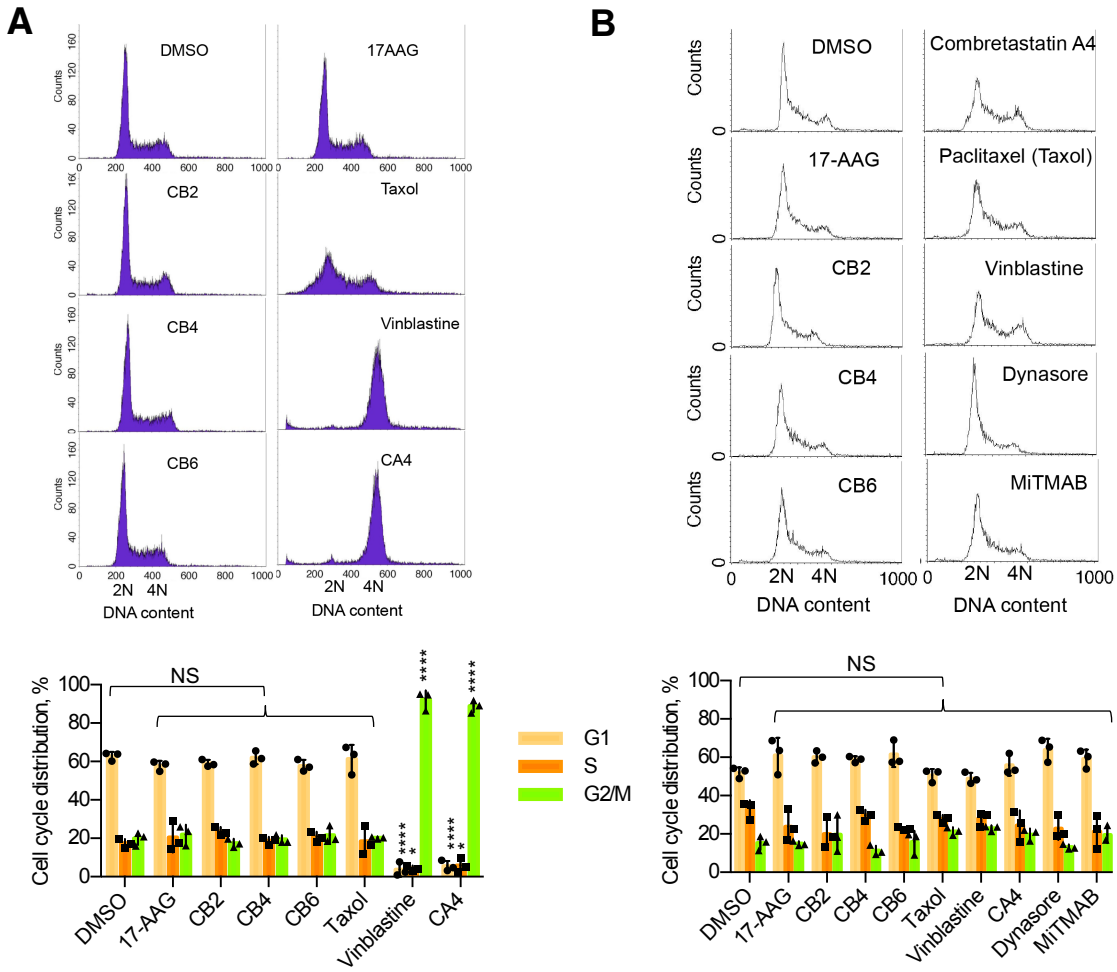


**Supplemental Figure 3. (A)** Cell cycle distribution following 16 hr treatment with tubulin binders. Control compound 17-AAG does not change cell cycle distribution. Tubulin binding compounds from the LY290181 family (CB2, CB4, and CB6) do not affect cell cycle distribution, while combretastatin A4 (CA4) and vinblastine show significant cell cycle changes. **(B)** 3 hr treatment with different compounds used in this study does not introduce changes in cell cycle distribution. (A, B) Top: representative FACS histograms. Bottom: estimation of fractions of cells in G1, S and G2/M phases of the cell cycle. Shown are means ± SDs from n = 3 measures within two experiments. Drug treatments were compared to the solvent only treatment. Differences are significant where shown. Significance analysis: ANOVA with Dunnett's post-hoc adjustments. *, $p < 0.05$, **, $p < 0.01$; ***, $p < 0.001$; ****, $p < 0.0001$.

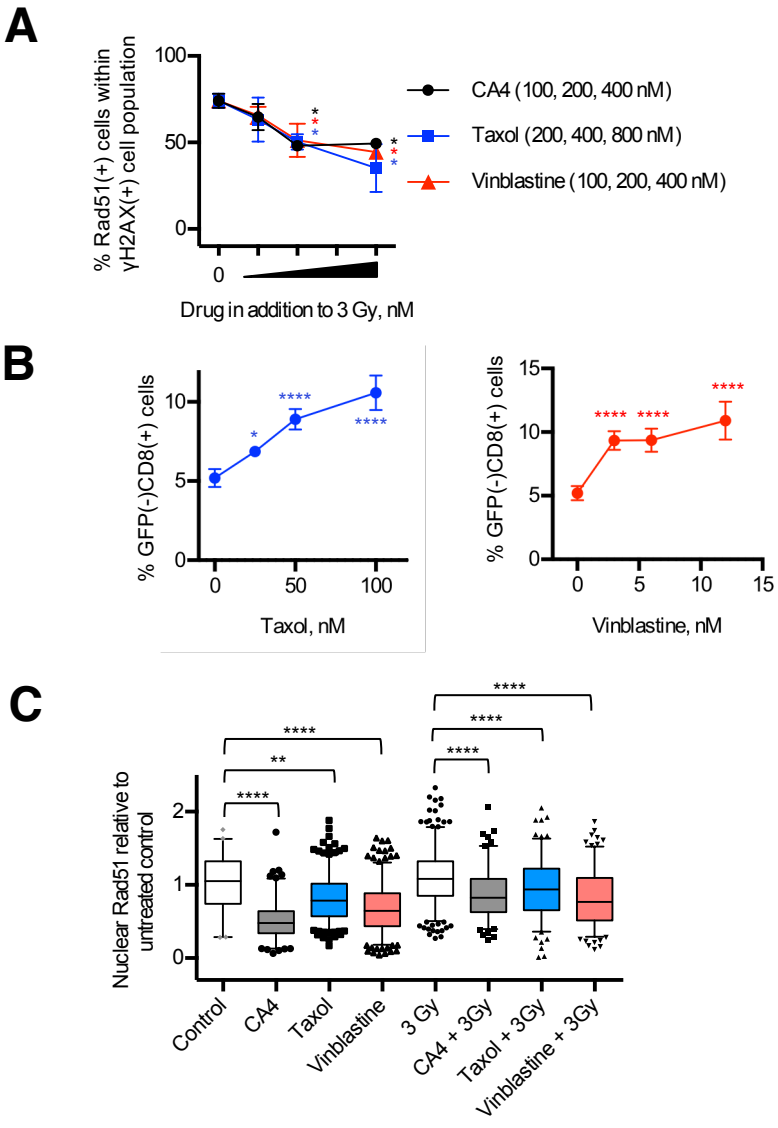


**Supplemental Figure 4. (A)** Dose-dependent inhibition of Rad51 focus formation by tubulin binders at DSB (γH2AX-positive) sites in CHO AA8 cells 2 hours post-IR with 3 Gy. **B)** Tubulin binders taxol and vinblastine do not inhibit non-homologous end joining (NHEJ), as measured by the appearance of GFP(-)CD8(+) cells within the 293-1040 cell population. Significant dose-dependent increase in NHEJ after treatment with tubulin binders can be explained by compensation for homologous recombination deficiency induced by tubulin binders. **(C)** Treatment with tubulin binders combretastatin A4 (CA4), taxol, and vinblastine reduces nuclear Rad51 levels both in non-irradiated and irradiated samples. Shown are values obtained by quantitating the Rad51 fluorescence signal in the nucleus. The boxes and whiskers contain points within $25^{th}$-$75^{th}$ and $5^{th}$-$95^{th}$ percentiles, respectively. Data from n ≥ 2 experiments. Significance analysis: ANOVA. Differences between tubulin binder-treated and non-treated samples are shown when significant. *, $p < 0.05$, **, $p < 0.01$; ***, $p < 0.001$; ****, $p < 0.0001$. NS = non-significant.

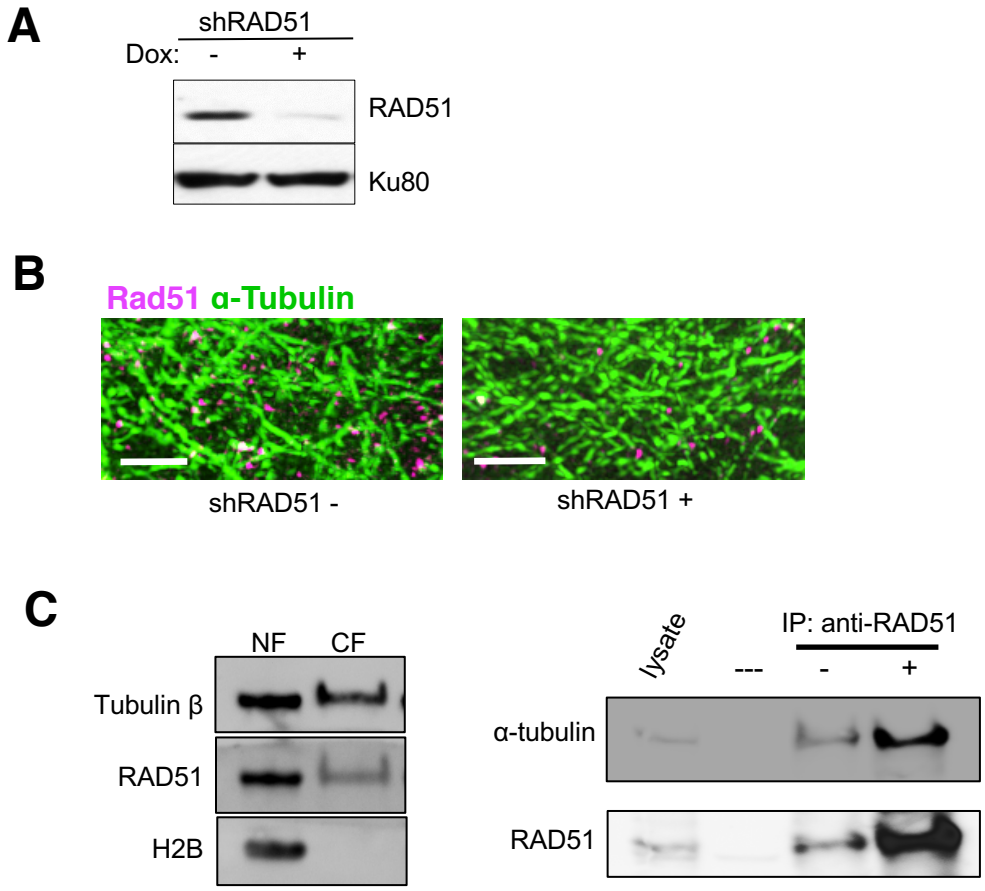


**Supplemental Figure 5. RAD51 is associated with tubulin.** (**A, B**) Super-resolution analysis shows that microtubule-associated RAD51-positive vesicles disappear after RAD51 knockdown. **(A)** RAD51 knockdown is induced in the HT1080-FUCCI cells that contain a doxycycline-inducible shRAD51 construct. Cells were incubated with 2 ug/ml doxycycline for 5 days. RAD51 knockdown was confirmed by western blotting using anti-RAD51 antibody. **(B)** The HT1080-FUCCI cells (day 5 after RAD51 knockdown) were stained with antibodies against alpha-tubulin and RAD51 and subjected to super-resolution microscopy analysis. Scale bar 2 μm. (**C**) Immunoprecipitation of RAD51 from cytoplasmic fraction of MDA-MB-231-BR3 cells reveals association with tubulin. Left panel: cell fractionation. NF = nuclear fraction, CF = cytoplasmic fraction. Note: Cell lysis was performed at room temperature to preserve microtubules. Since the tubulin is in polymerized form it may be attached to the surface of the nucleus, explaining the appearance of tubulin in the NF. Right panel: immunoprecipitation.

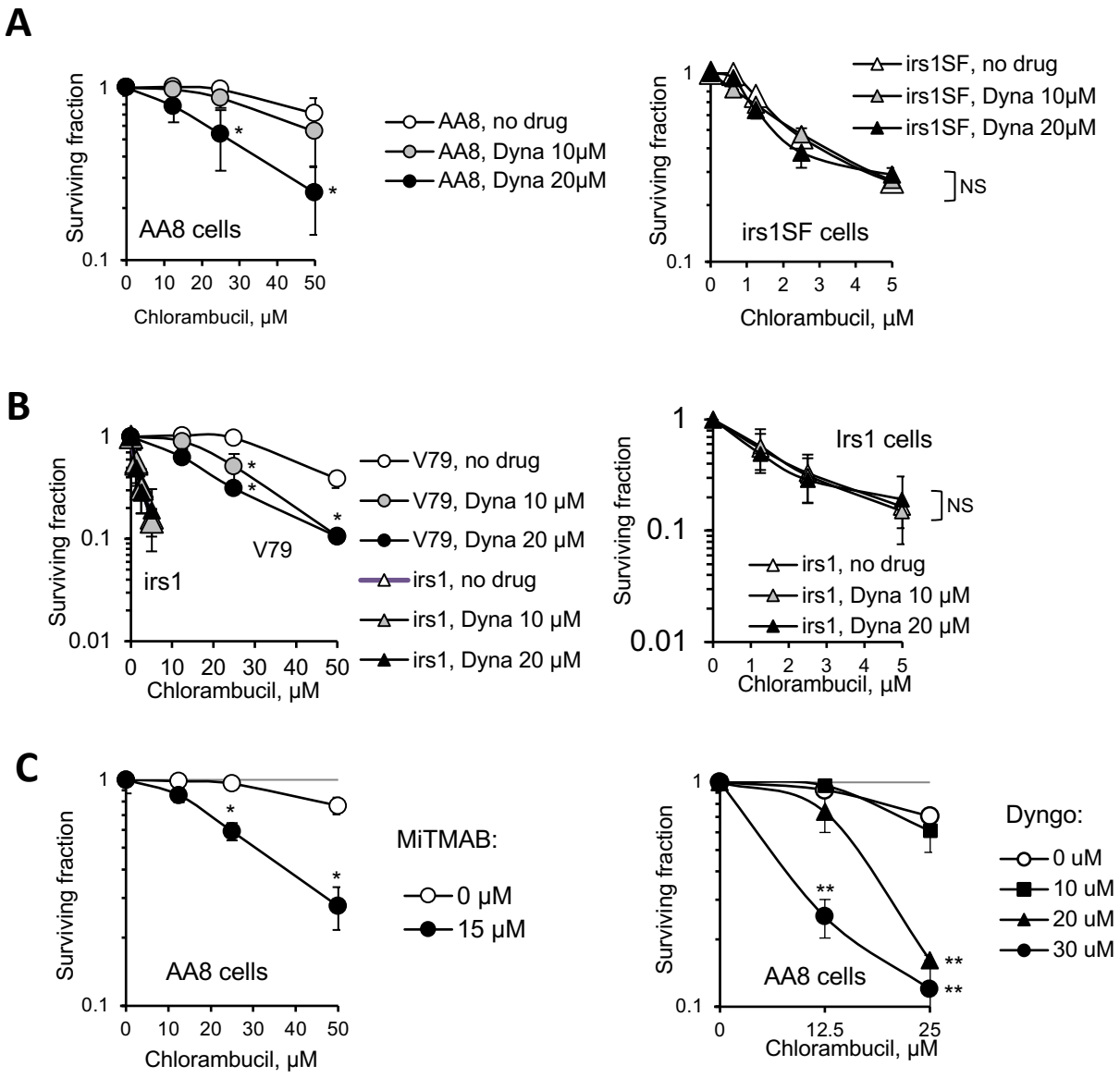


**Supplemental Figure 6. Dynamin inhibitors increase sensitivity to a DNA crosslinking agent chlorambucil in homology-directed repair (HDR)-proficient cells, but fail to sensitize HDR-deficient cells. (A, B)** Same data as in Figure 5F. Cells deficient in HDR proteins XRCC3 (irs1SF) and XRCC2 (irs1) are not sensitized to a DNA cross-linking agent chlorambucil by dynasore, while dynasore has a strong sensitizing effect on HDR-proficient cells AA8 and V79. Right graphs supplement Figure 5F showing irs1SF cell survival at very low doses of chlorambucil. **(B)** Dynasore increases sensitivity of V79 cells to chlorambucil, but does not increase sensitivity of HR-deficient irs1 cells. Right graph shows irs1 cell survival at very low doses of chlorambucil. **(C)** Dynamin 2 inhibitors MiTMAB and Dyngo increase sensitivity of CHO AA8 cells. Shown are means ± SDs (ranges) from n ≥ 2 MTS assays. Significance analysis: ANOVA. *, p <0.05, **, p < 0.01; ***, p < 0.001; ****, p < 0.0001. NS = non-significant.

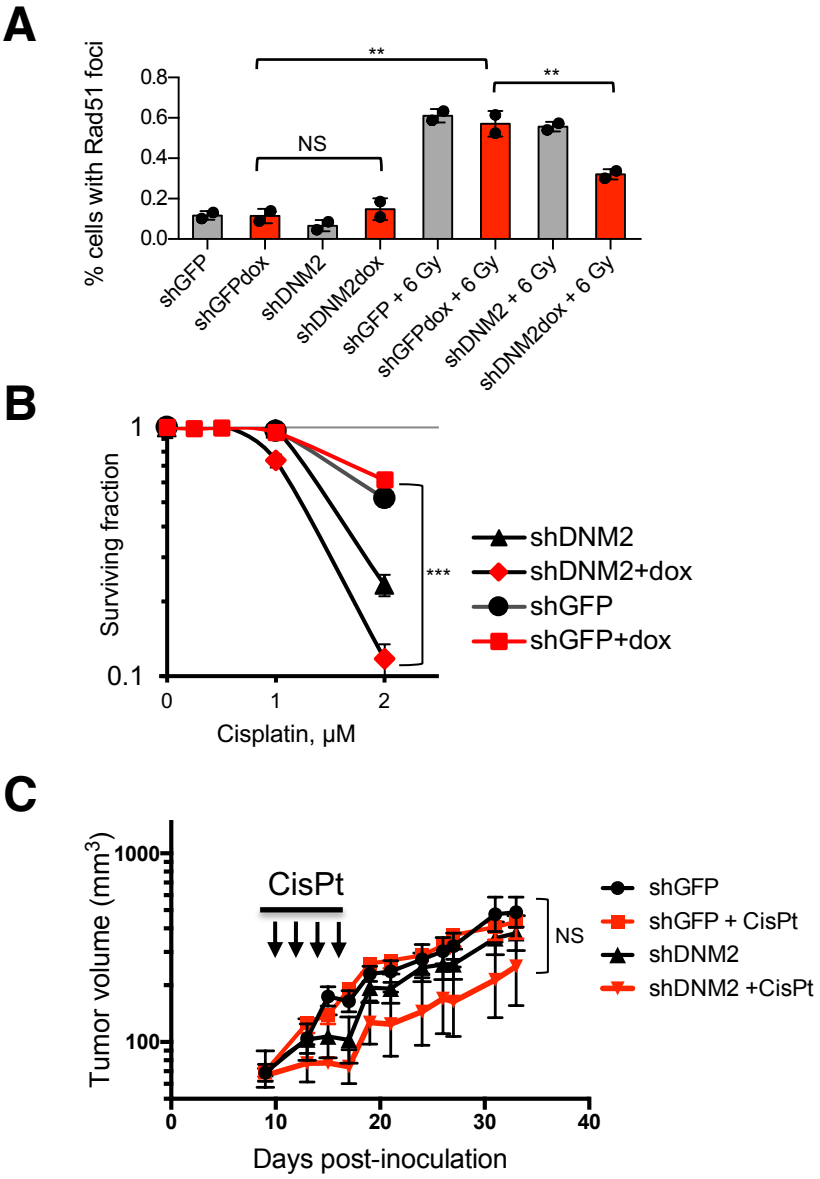


**Supplemental Figure 7.** Effects of dynamin 2 (DNM2) knockdown in triple-negative breast cancer MDA-MB-231-BR3 cells. DNM2 knockdown results in impaired formation of IR-induced Rad51 foci, increased cell sensitivity to cisplatin and a marginal, non-significant, potentiation of cisplatin effect on tumor growth. (**A**) DNM2 knockdown in human triple-negative breast cancer MDA-MB-231-BR cells was initiated by the addition of 2 μg/ml doxycycline (see the Western blot in Figure 5F). On day 5 of doxycycline treatment cells were irradiated with 6 Gy and % of cells with Rad51 foci was estimated by immunofluorescence. Shown are means and ranges from two separate experiments. In each experiment, 50-150 cells were counted per sample. Significance test: ANOVA. (**B**) shDNM2 knockdown increases sensitivity to cisplatin in the MDA-MB-231-BR3 cells. Shown are means ± ranges from two separate MTS assays done in triplicate. Note: an increased sensitivity in the shDNM2 group is caused by partial knockdown of DNM2. Significance analysis: ANOVA. (**C**) DNM2 knockdown increases sensitivity to cisplatin, but the effect is not significant. Cisplatin was given at 4 mg/kg on days 11, 13, 15, and 17. This regimen of cisplatin administration caused significant reduction of mouse body weight due to toxicity during treatment (not shown).

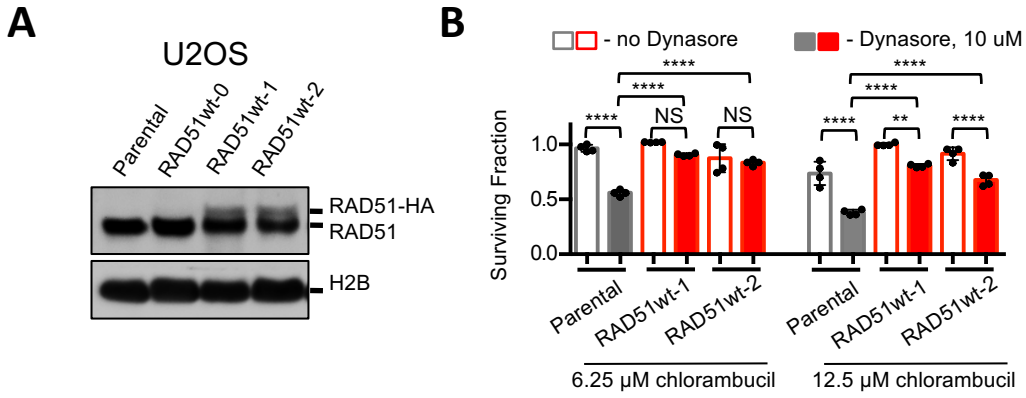


**Supplemental Figure 8. (**This figure supplements Figure 6). **Overexpression of RAD51 rescues dynasore-induced sensitization to chlorambucil in U2OS cells. (A)** Western blot shows RAD51 levels in two separate cell populations overexpressing wild-type RAD51-HA (RAD51wt-1 and RAD51wt-2). **(B)** Overexpression of RAD51 rescues dynasore-induced sensitization to chlorambucil in two separate populations of RAD51-overexpressing cells. MTS assays: shown are means and SDs from n > 2 experiments. Significance analysis: ANOVA. *, $p < 0.05$, **, $p < 0.01$, ***, $p < 0.001$; ****, $p < 0.0001$. NS = not significant.

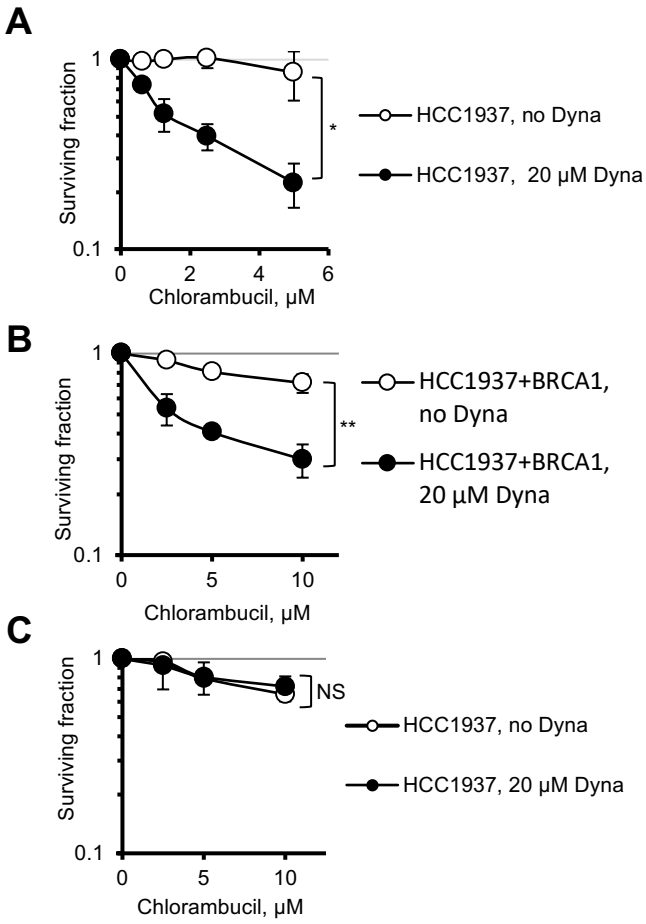


**Supplemental Figure 9. BRCA1-mutant and BRCA1-corrected cells are sensitized to chlorambucil by inhibition of dynamin.** A well characterized BRCA1-mutant triple-negative breast cancer cell line HCC1937 bearing an empty pcDNA3.1 plasmid (A) and its derivative bearing BRCA1-expressing plasmid (B) (63, 64) were both sensitized to chlorambucil by dynasore. We would like to note that one subpopulation of HCC1937 cells (C) obtained from a different source did not respond to dynasore treatment. Shown are means ± SDs from n ≥ 3 MTS assays. Significance analysis: two-way ANOVA. *, $p < 0.05$, **, $p < 0.01$; NS = not significant.

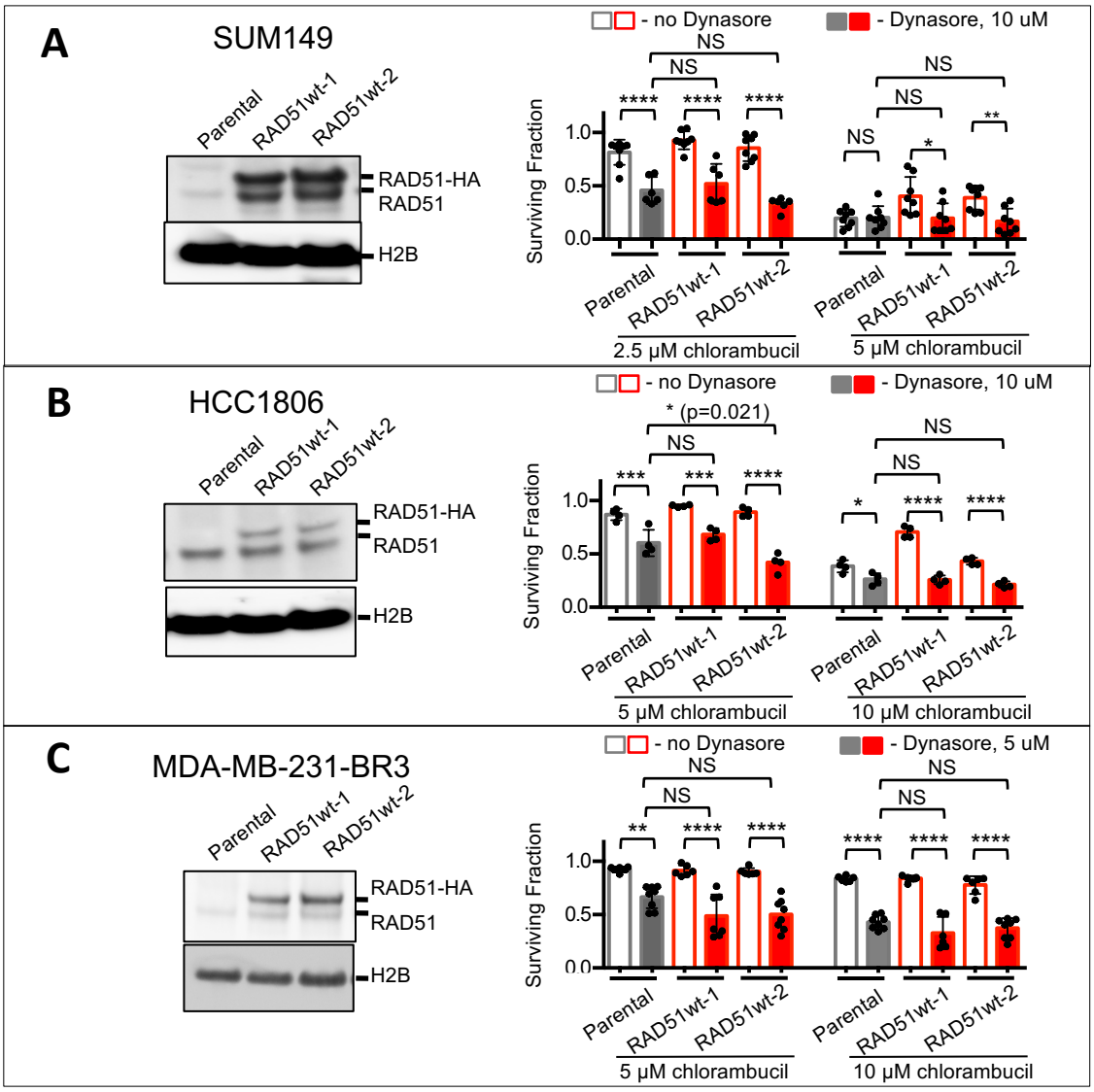


**Supplemental Figure 10.** (This figure supplements Figure 7)**. Overexpression of RAD51 fails to rescue dynasore-induced sensitization to chlorambucil in triple-negative breast cancer cells. (A-C)** Left panels: Western blots show RAD51 levels in two separate cell populations overexpressing wild-type RAD51-HA (RAD51wt-1 and RAD51wt-2). Right panels: Overexpression of RAD51 in TNBC cells does not rescue dynasore-induced sensitization to chlorambucil. Significance analysis using two separate populations of RAD51-transfected cells. MTS assays: shown are means and SDs from n > 2 experiments. (A-C) Rescue experiments performed in TNBC cell lines: BRCA1-mutant SUM149 (B), and BRCA1 wild-type HCC1806 (C) and MDA-MB-231-BR3 (D). Significance analysis: ANOVA. *, $p < 0.05$, **, $p < 0.01$, ***, $p < 0.001$; ****, $p < 0.0001$. NS = not significant.

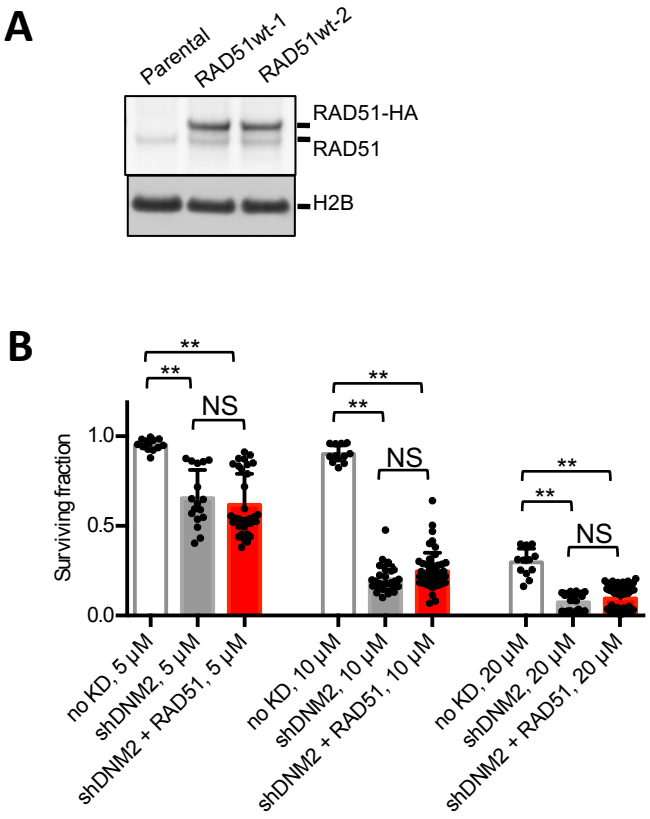


**Supplemental Figure 11. Overexpression of RAD51 fails to rescue sensitization to chlorambucil caused by knockdown of DNM2 in triple-negative MDA-MB-231-BR3 breast cancer cells.** This figure supplements Figure 7E of the manuscript. **(A)** Western blots show RAD51 levels in the MDA-MB-231-BR3 cell line with doxycycline inducible knockdown of DNM2. Shown are two separate cell populations overexpressing wild-type RAD51-HA (RAD51wt-1 and RAD51wt-2). **(B)** MTS assays showing the points that made into the mean values on the graph in Figure 7E. Shown are means and SDs from n ≥ 3 experiments. Significance analysis: ANOVA. **, $p < 0.01$. NS = not significant.

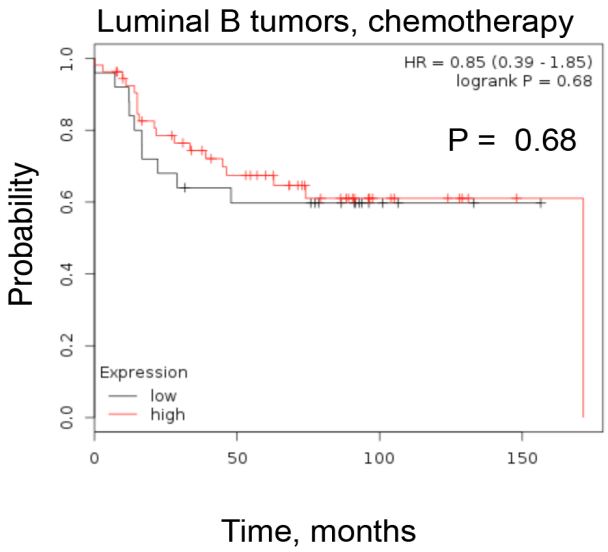


**Supplemental Figure 12**. Dynamin 2 (*DNM2*) expression does not affect chemotherapy outcome for patients with estrogen receptor-positive, luminal B, breast cancers. Kaplan-Meier analysis of breast cancer patients with chemotherapy-treated estrogen receptor (ER)-positive luminal B breast tumors treated with chemotherapy. Patients were split by median expression of *DNM2* over the entire breast cancer dataset (3455 patients). Patients with higher than median expression of *DNM2* are denoted in red, and with lower than median expression of DNM2 – in black.

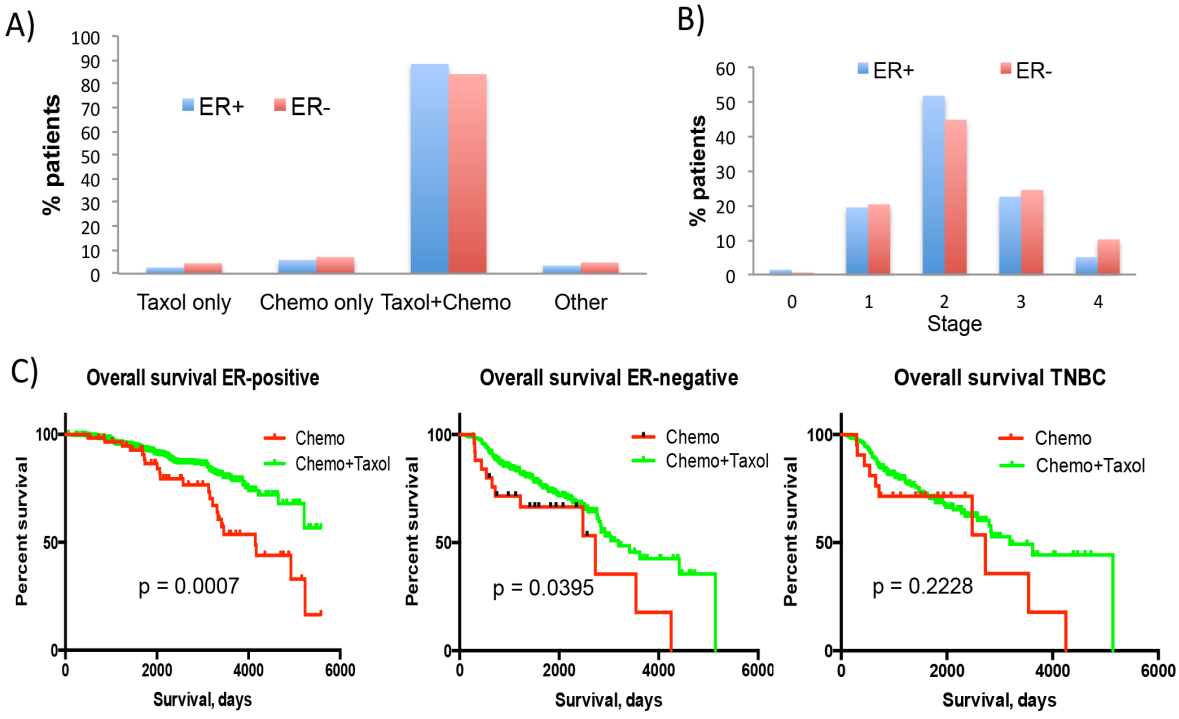


**Supplemental Figure 13.** Data from the Stanford Cancer Institute Research Database show that in this group of patients there is no difference in (**A**) taxol usage and (**B**) stage distribution between estrogen receptor (ER)-positive and ER-negative groups of breast cancer patients treated with DNA-damaging chemotherapy. (**C**) ER-positive breast cancer patients benefit from the addition of taxol to chemotherapy. Significance: Mantel-Cox test. In contrast, there is no significant benefit of taxol addition to the cytotoxic therapy in the triple-negative breast cancer (TNBC) cohort.

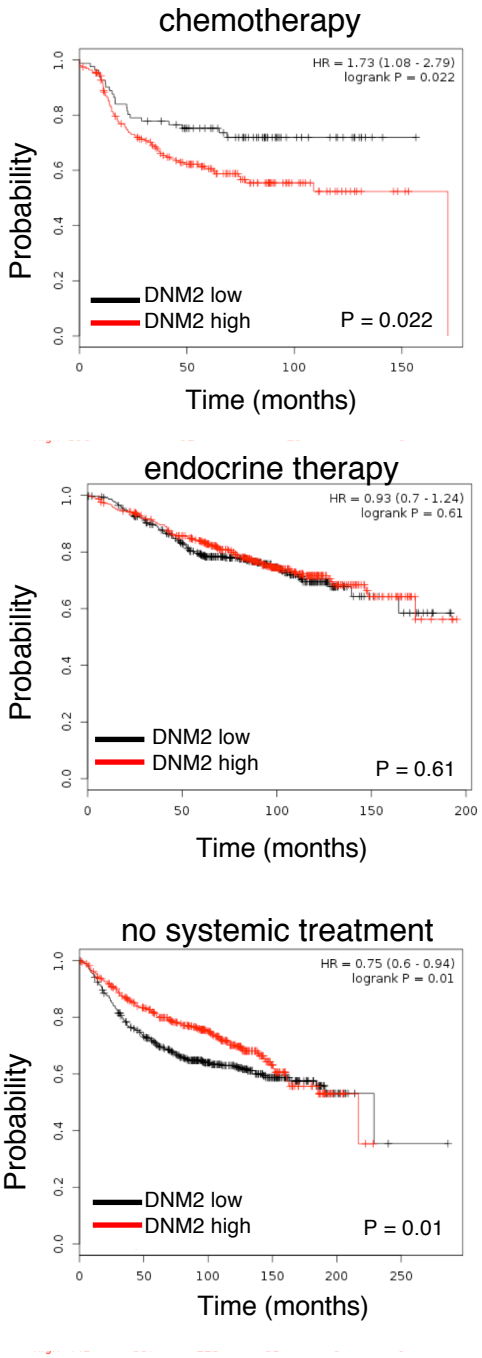


**Supplemental Figure 14. Dynamin 2 (*DNM2*) expression determines chemotherapy outcome for breast cancer patients. (A**) Kaplan-Meier analysis on 1000 systemically untreated patients, 752 patients treated with endocrine therapy and 274 breast cancer patients treated with chemotherapy. Patients were split by median expression of *DNM2* over the entire breast cancer dataset (3455 patients). Patients with higher than median expression of *DNM2* are denoted in red, and with lower than median expression of *DNM2* – in black.

**Supplemental Table 1. DNM2 knockdown (shDNM2) increases tumor sensitivity to cyclophosphamide (CPX) in an orthotopic model of triple-negative breast cancer.** The knockdown of DNM2 results in a synergistic increase in tumor sensitivity to CPX, while the effect of CPX alone is not significant. Shown is a statistical analysis for the experiment from Figure 8C. The data were analyzed in a linear mixed effects model to account for the within mouse correlation. Post hoc pair-wise comparisons were performed using a Tukey adjustment for multiple comparisons. Analysis for the days 35, 45, 47, and 49 are shown below.

| Effect | Group | Group | Day | Estimate | pvalue |
|---|---|---|---|---|---|
| Group | Control | Control+CPX | 35.00 | 0.1677 | 0.2826 |
| Group | Control | shDNM2 | 35.00 | 0.05198 | 0.9312 |
| Group | Control | shDNM2 +CPX | **35.00** | **0.4439** | **<.0001** |
| Group | Control+CPX | shDNM2 | 35.00 | -0.1158 | 0.5684 |
| Group | Control+CPX | shDNM2 +CPX | 35.00 | 0.2761 | 0.0142 |
| Group | shDNM2 | shDNM2 +CPX | **35.00** | **0.3919** | **<.0001** |

| Effect | Group | Group | Day | Estimate | pvalue |
|---|---|---|---|---|---|
| Group | Control | Control+CPX | 45.00 | 0.2781 | 0.1008 |
| Group | Control | shDNM2 | 45.00 | 0.1455 | 0.5577 |
| Group | Control | shDNM2 +CPX | **45.00** | **0.5661** | **<.0001** |
| Group | Control+CPX | shDNM2 | 45.00 | -0.1326 | 0.6597 |
| Group | Control+CPX | shDNM2 +CPX | 45.00 | 0.2880 | 0.0710 |
| Group | shDNM2 | shDNM2 +CPX | **45.00** | **0.4206** | **0.0006** |

| Effect | Group | Group | Day | Estimate | pvalue |
|---|---|---|---|---|---|
| Group | Control | Control+CPX | 47.00 | 0.3062 | 0.0788 |
| Group | Control | shDNM2 | 47.00 | 0.1693 | 0.4711 |
| Group | Control | shDNM2 +CPX | **47.00** | **0.5909** | **<.0001** |
| Group | Control+CPX | shDNM2 | 47.00 | -0.1368 | 0.6745 |
| Group | Control+CPX | shDNM2 +CPX | 47.00 | 0.2847 | 0.1019 |
| Group | shDNM2 | shDNM2 +CPX | **47.00** | **0.4215** | **0.0013** |

| Effect | Group | Group | Day | Estimate | pvalue |
|---|---|---|---|---|---|
| Group | Control | Control+CPX | 49.00 | 0.3363 | 0.0618 |
| Group | Control | shDNM2 | 49.00 | 0.1950 | 0.3922 |
| Group | Control | shDNM2 +CPX | **49.00** | **0.6158** | **<.0001** |
| Group | Control+CPX | shDNM2 | 49.00 | -0.1413 | 0.6892 |
| Group | Control+CPX | shDNM2 +CPX | 49.00 | 0.2795 | 0.1450 |
| Group | shDNM2 | shDNM2 +CPX | **49.00** | **0.4208** | **0.0026** |

Gel for the Figure 5F

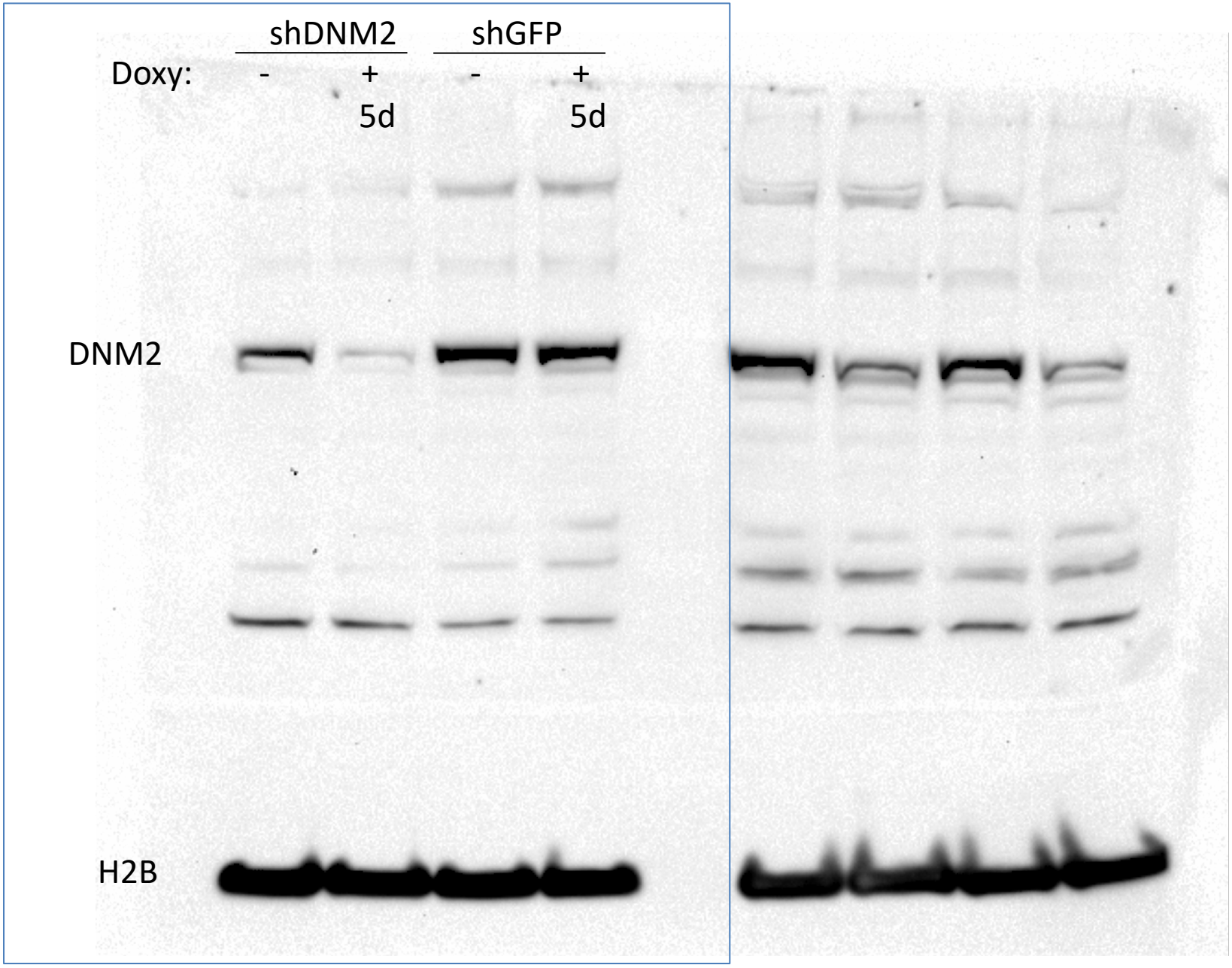


Membrane was cut in two and the upper part was incubated with anti-DNM2 antibody and the lower part was incubated with anti-H2B antibody.

Gel for the Supplemental Figure 5A

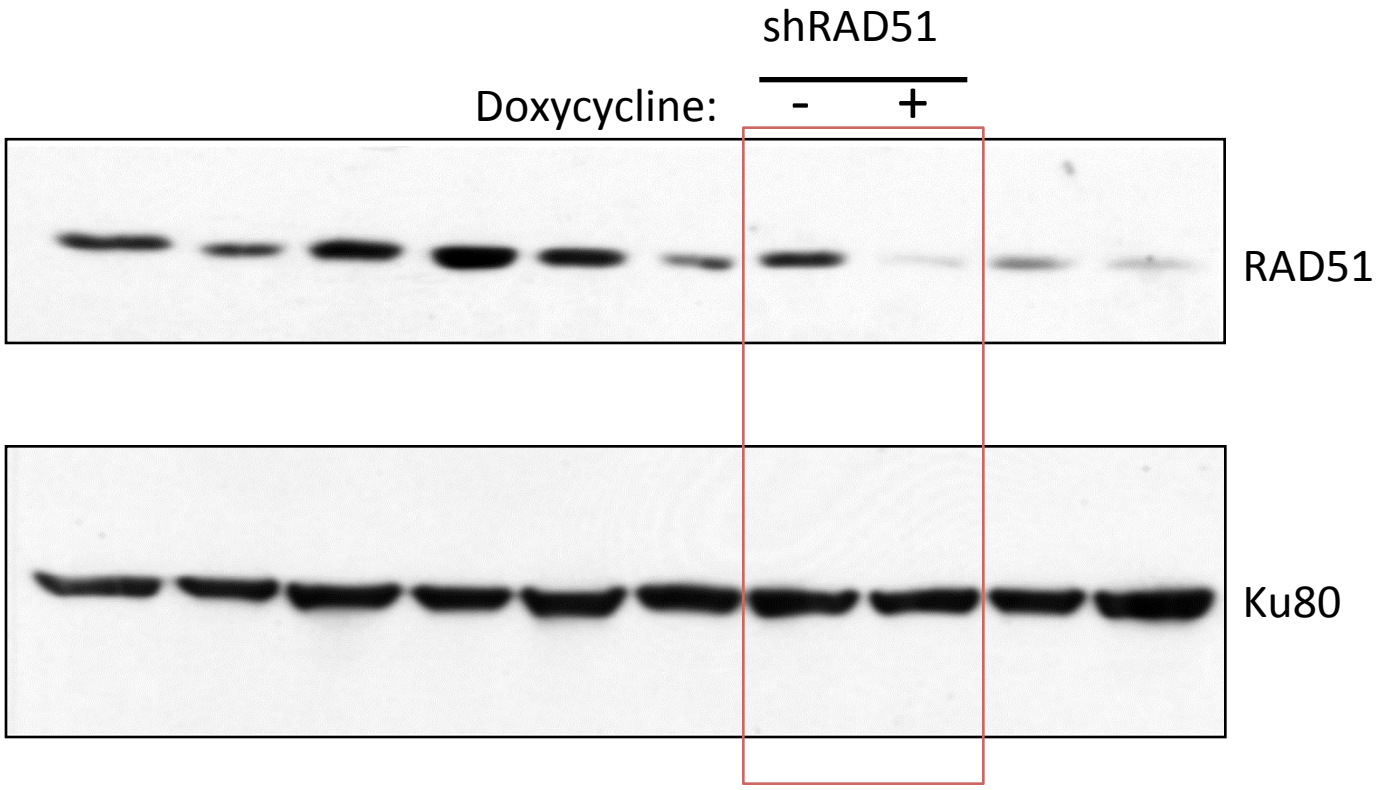


Membrane was cut in two and one (lower) part was incubated with anti-RAD51 and another (top) with anti-KU80 antibodies

Gel for the Supplemental Figure 5C (left)

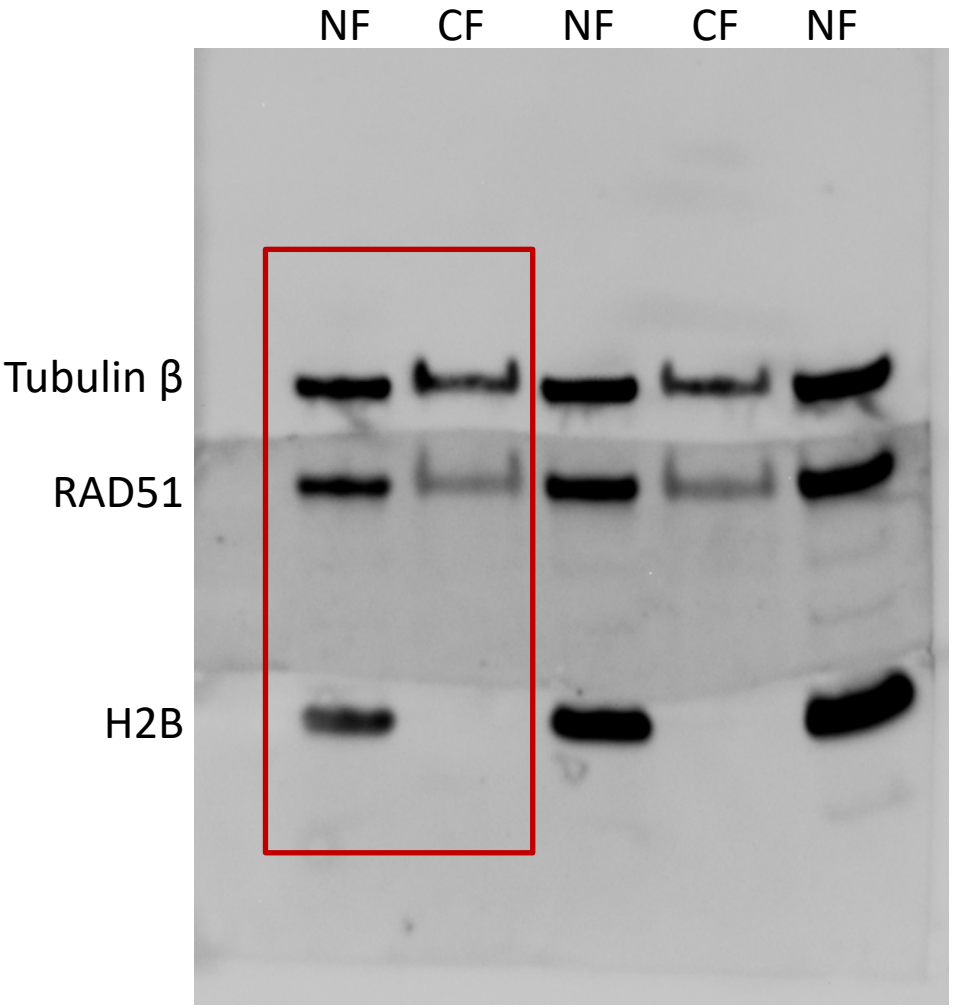


Membrane was cut in three and the parts were incubated with anti-Rad51, anti-tubulin and anti-histone H2B antibodies

Gels for the Supplemental Figure 5C

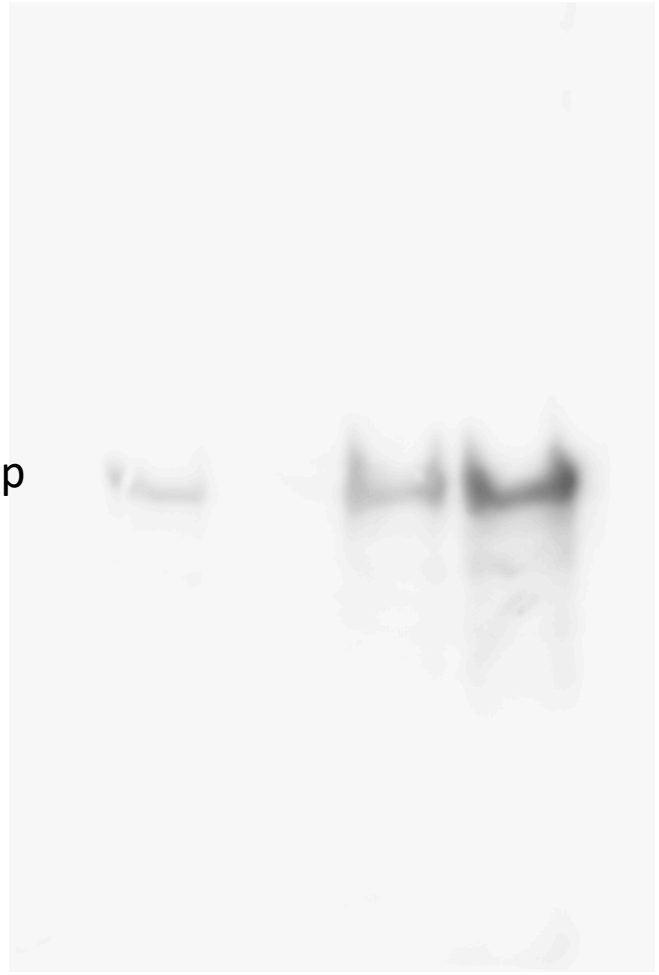

TUB-hrp

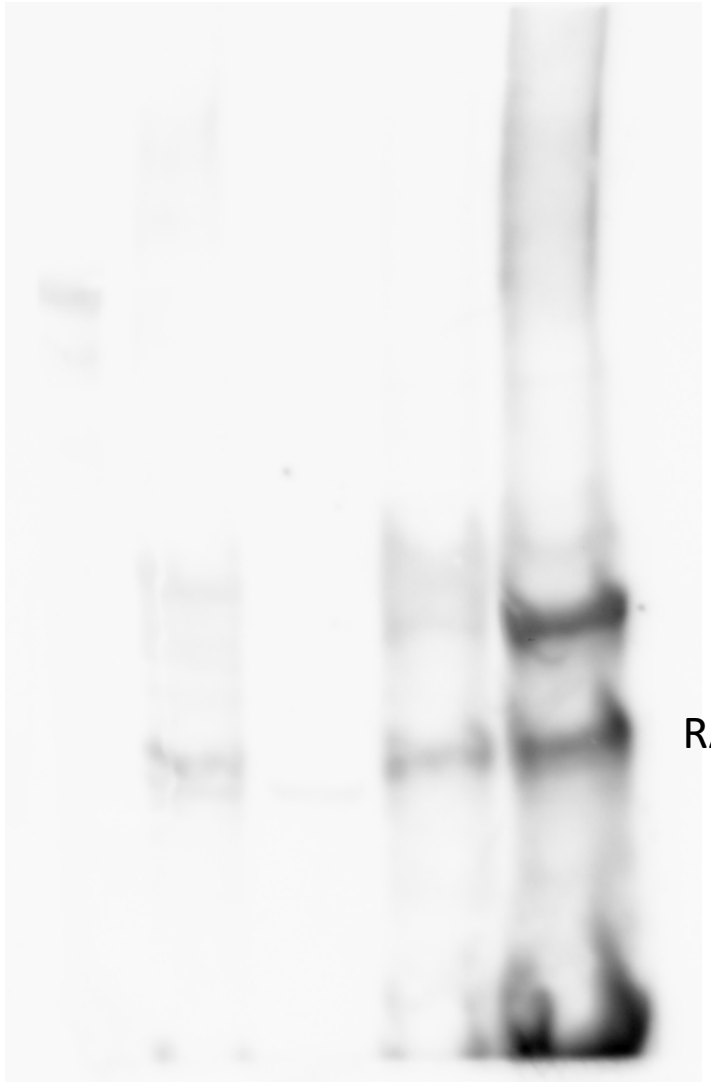

RAD51

Membrane was cut in two and the part used for the immunoprecipitation experiment was incubated with anti-Rad51 and anti-tubulin-hrp antibodies

# Gel for Supplemental Figure 8A

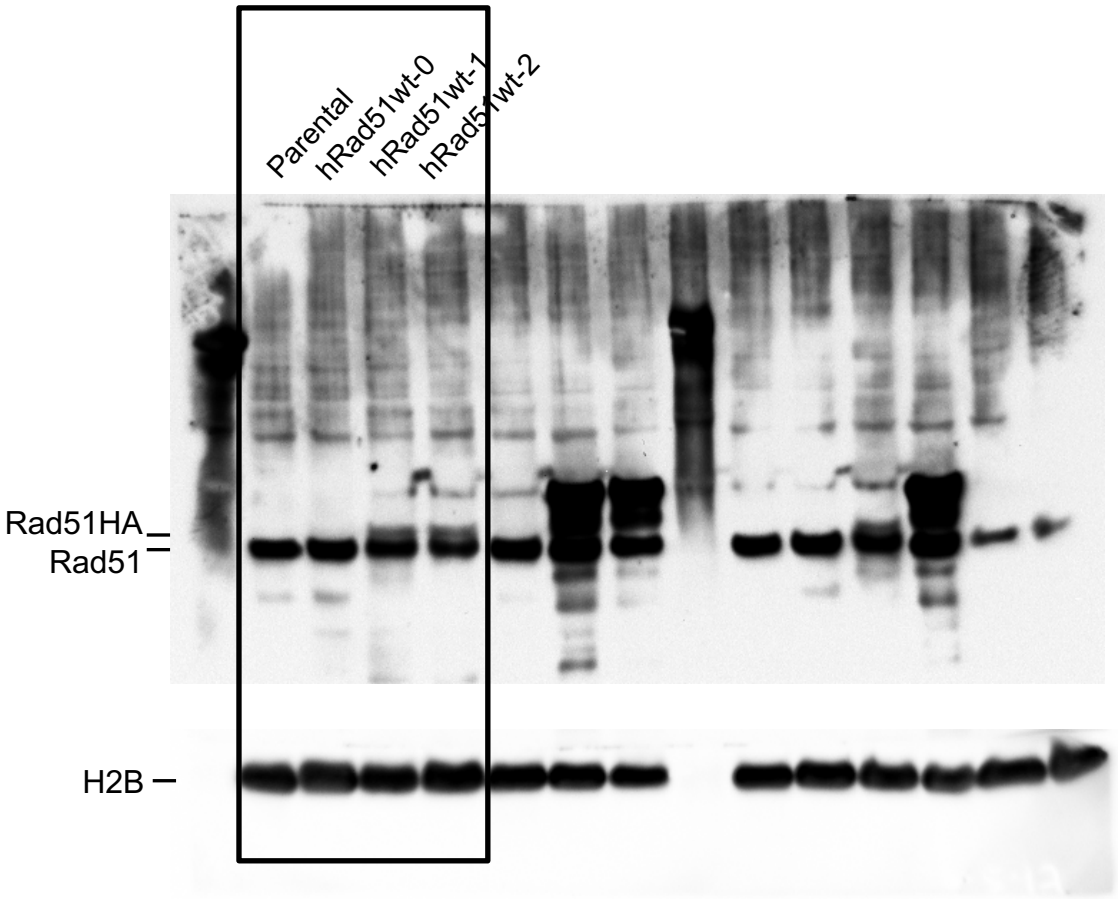


Membrane was cut in two and the upper part was incubated with anti-Rad51 and anti-HA antibodies and the lower part was incubated with anti-H2B antibody.

Gel for Supplemental Figure 10A

Gel for Supplemental Figure 10B

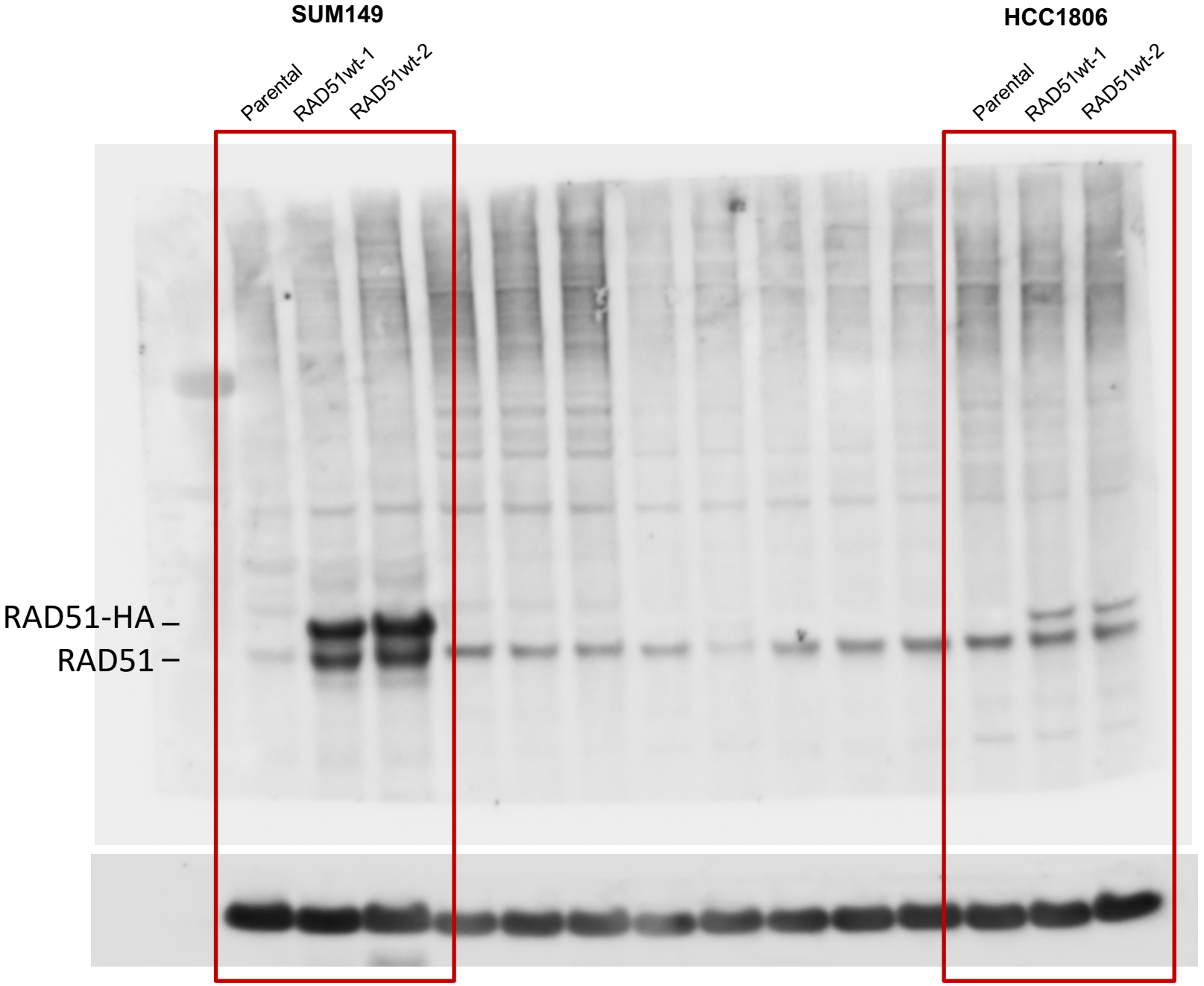

Gels for Supplemental Figures 10C and 11A

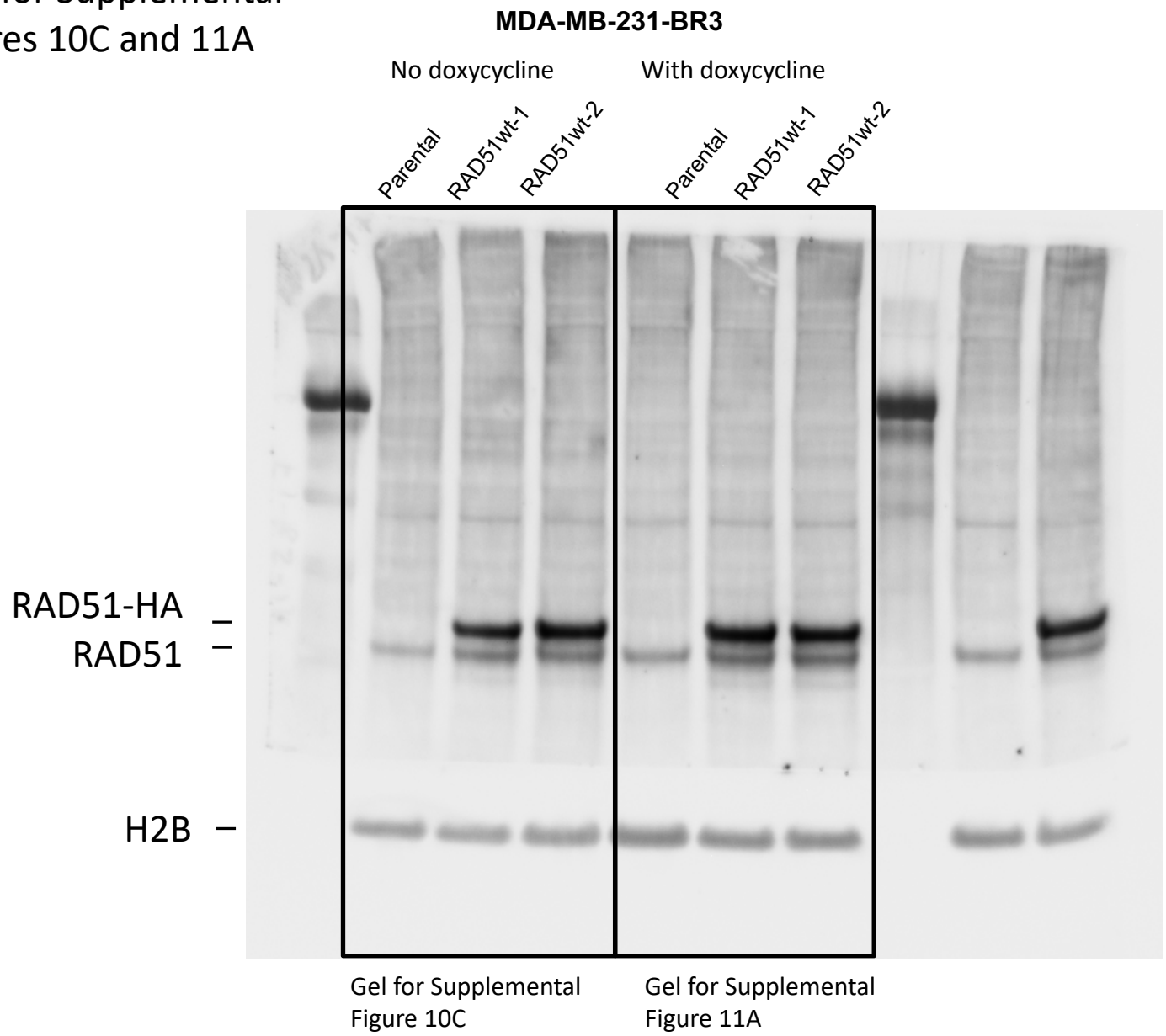


The membrane was cut in two and one (lower) part was incubated with anti-H2B and another (top) with anti-RAD51 and anti-HA antibodies